[Journal of Geophysical Research: Solid Earth]

Supporting Information for

Sub-decadal Volcanic Tsunamis Due to Submarine Trapdoor Faulting at Sumisu Caldera in the Izu-Bonin Arc

Osamu Sandanbata,[1,2†] Shingo Watada,[1] Kenji Satake,[1] Hiroo Kanamori,[3] Luis Rivera,[4] and Zhongwen Zhan[3]

[1]Earthquake Research Institute, the University of Tokyo, Bunkyo, Tokyo, Japan.

[2]National Research Institute for Earth Science and Disaster Resilience, Tsukuba, Ibaraki, Japan.

[3]Seismological Laboratory, California Institute of Technology, Pasadena, CA 91125, USA.

[4]Université de Strasbourg, CNRS, ITES UMR 7063, Strasbourg F-67084, France.

Corresponding author: Osamu Sandanbata (osm3@bosai.go.jp)

Contents of this file

Additional Supporting Information (Files uploaded separately)

Captions for Data Set S1

Introduction

Supporting information contains descriptions of procedures for the moment tensor analysis (Text S1), and source model variations when we assume low-velocity layer in the crust (Text S2) or non-uniform dip angle of the ring fault (Text S3). Supplementary figures and tables mentioned in Main Text (Figures S1 to S8; Tables S1 to S3), and a caption for the supplementary dataset of the source models (Data set S1), are also contained.

Text S1. Moment tensor analysis

We perform the deviatoric moment tensor analysis using the W-phase of seismic waves (Kanamori and Rivera 2008; Duputel et al. 2012; Hayes, Rivera, and Kanamori 2009) for the four earthquakes in 1996, 2006, 2015, and 2018 at Sumisu caldera; we do not analyze the 1984 event, due to inaccessibility of good quality seismic data. We download broad-band seismic records of F-net and/or GSN within the epicentral distances of 30°. We use the same Green's functions of seismic waveforms, the same filter, and assume the same centroid location, as done for the computation of the long-period seismic waveforms in Main Text (see Section 4.3). We assume the zero-trace condition $M_{rr} + M_{\theta\theta} + M_{\phi\phi} = 0$. The optimum time-shift and half duration are assumed to be the same and determined by the grid-search method. In the inversion process, we remove clearly bad records yielding a single-record seismic misfit larger than 1.5 (Table S2). The estimated deviatoric moment tensors are shown in Table S3.

From the deviatoric moment tensors, we obtain the *resolvable moment tensors* $\boldsymbol{M_{res}}$, by excluding two elements $M_{r\theta}$ and $M_{r\phi}$ that are indeterminate from long-period seismic data (Sandanbata et al. 2021). $\boldsymbol{M_{res}}$ of the four earthquakes are shown in Figure 8a. Following our previous study (Sandanbata et al. 2021), we examine the dominancy of the vertical-CLVD component (denoted by k_{CLVD}) and the null-axis direction (denoted by the best-fit double-couple orientation) of $\boldsymbol{M_{res}}$. Since the two parameters are controlled by the ring fault arc length and orientation, comparisons of those for the repeating earthquakes enable us to evaluate similarities in their ring fault geometries (See Section 6.3).

Text S2. Effect of a low-rigidity crust on our estimation of the ring fault dip angle

In the source modeling in Main Text, we estimated the ring fault dip angle as 85.0°, by utilizing the sensitivity of the long-period seismic amplitudes to the parameter, when we used the velocity model with V_p = 6.0 km/s, V_s = 3.5 km/s, respectively and ρ_0 = 2.6 x 10^3 kg/m^3 in the shallowest crust at < 15 km depth, and assumed the Lamé's constants of λ = 29.9 GPa and μ = 31.85 GPa (see Section 4.3). However, a previous study (Kodaira et al. 2007) suggested a lower-velocity layer with V_p of 1.8–5.8 km/s exists in the shallowest depth < ~5 km of the Izu-Bonin arc, including the region around Sumisu caldera. The low velocity, or low rigidity, at the source may reduce the seismic amplitude and thereby affect our estimate of the ring fault dip angle. Here, we recompute long-period seismic waveforms from the source models with a ring fault with different uniform dip angles along the two-third ring arc length, using a modified velocity model with a lower-velocity layer with V_p = 3.87 km/s, V_s = 2.24 km/s, ρ_0 = 2.0 x 10^3 kg/m^3 in depth < 5 km. Based on the values, the Lamé's constants are $\lambda = \mu$ = 10.0 GPa for the moment tensor computation. Figure S7 demonstrates that the model with 77° yields the best agreement with the observed seismic amplitude. Thus, if we assume the value of λ and μ ranging from 10 GPa to ~30 GPa in the shallowest crust, our estimation of the ring fault dip angle ranges from ~77° to ~85°.

Text S3. Source model with modification of the ring fault dip angle

For an additional analysis, we perform the same earthquake source modeling procedures (see Section 4) for a source structure containing a ring fault along the two-third ring arc length with *nonuniform dip angles* that decrease from 87° on the northeastern part to 83° on the two ends (Figure S8a). The source model with this structure (Figure S8), inverted from the tsunami waveform data, yields even better seismic waveform fit with a smaller misfit of 0.414 (Figure S8d) than the best-fit source model with the uniform ring fault dip angle (seismic misfit of 0.432; Figure 6c); for example, the waveform fits of the BHE channel of KZS, YMZ, TYS, and AMM are improved by the minimal parameter tuning. We use this model in Section 6.2 to discuss seismic radiations from the trapdoor faulting.

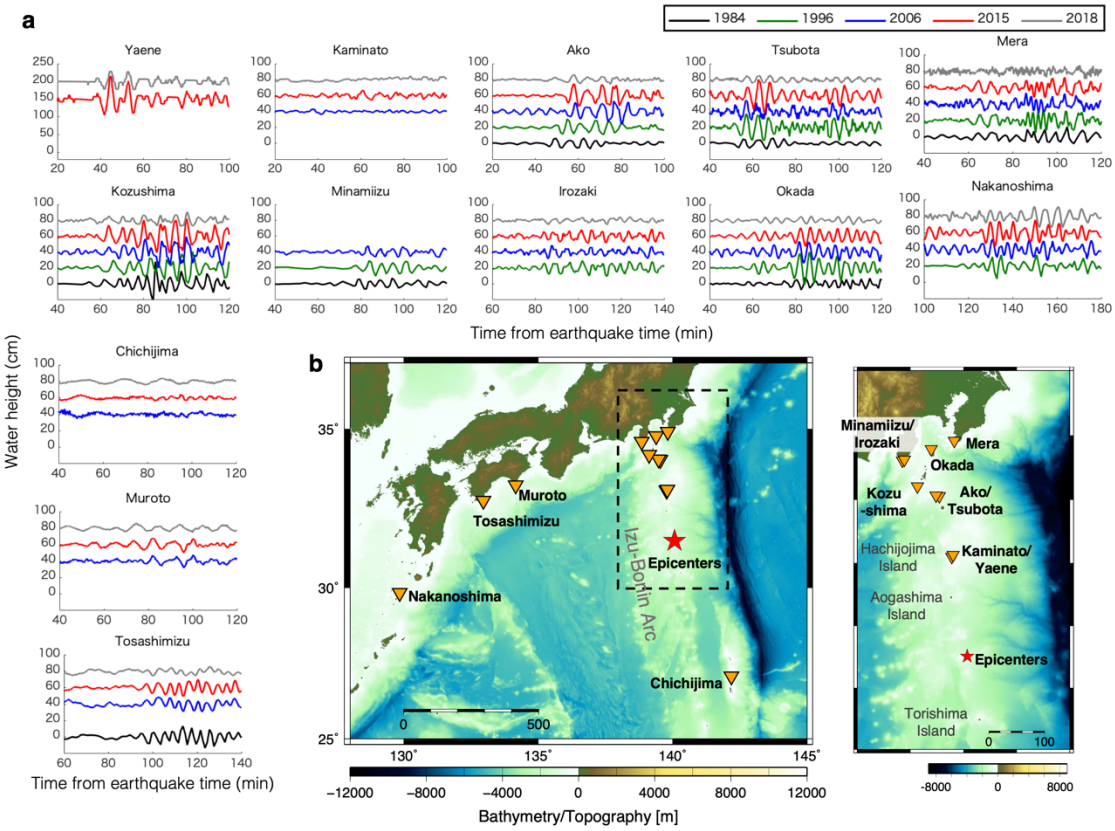

Figure S1. (**a**) Tsunami waveforms from the repeating earthquakes recorded by (**b**) tide gauge stations. In (**a**), base lines for different events are shifted by multiples of 50 cm and 20 cm in the y-axis direction for Yaene and the others, respectively. We remove the tidal trends from the raw data by the polynomial fitting. We additionally apply a band-pass filter (0.001-0.01 Hz) to the records of Tosashimizu and Chichijima to remove noise. Some records of the 1984 and 1996 events are digitized from analogue records.

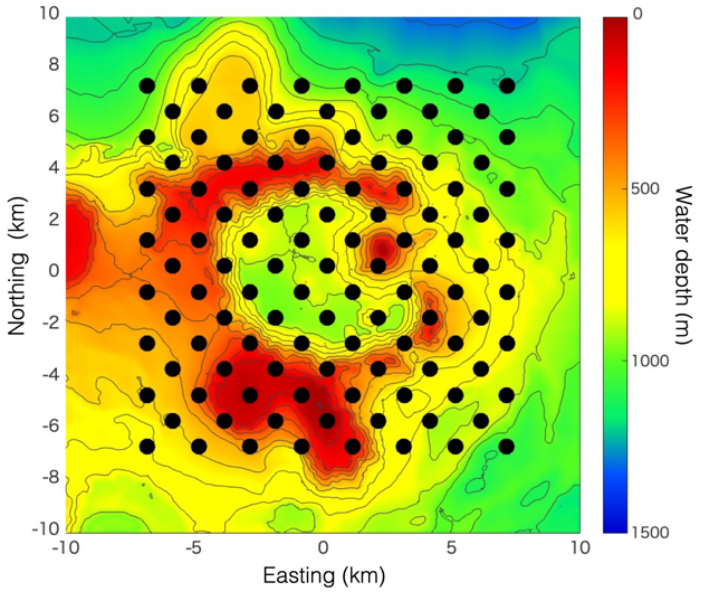

Figure S2. Unit sources of sea-surface displacement. Black dots represent central locations of 113 unit sources on the sea surface to compute the synthetic tsunami waveforms $\boldsymbol{g_j^k}$; each unit source has a cosine-tapered shape with a horizontal source size of 4 km x 4 km (Equation 1).

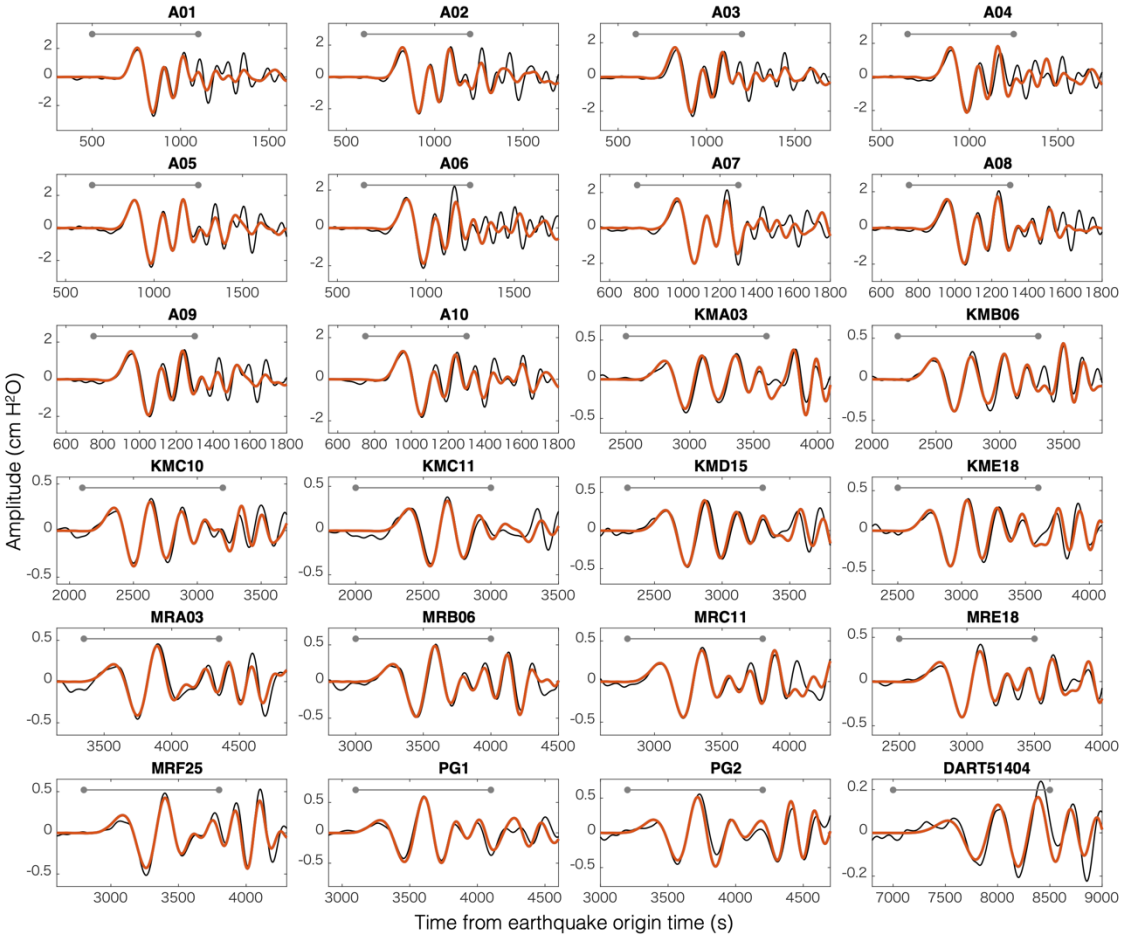

Figure S3. Comparison of the observed (black) and synthetic (red) tsunami waveforms at the OBP gauges from the initial sea-surface displacement model with uplift and subsidence (Figure 2a). The gray line represents the time interval used for the inversion.

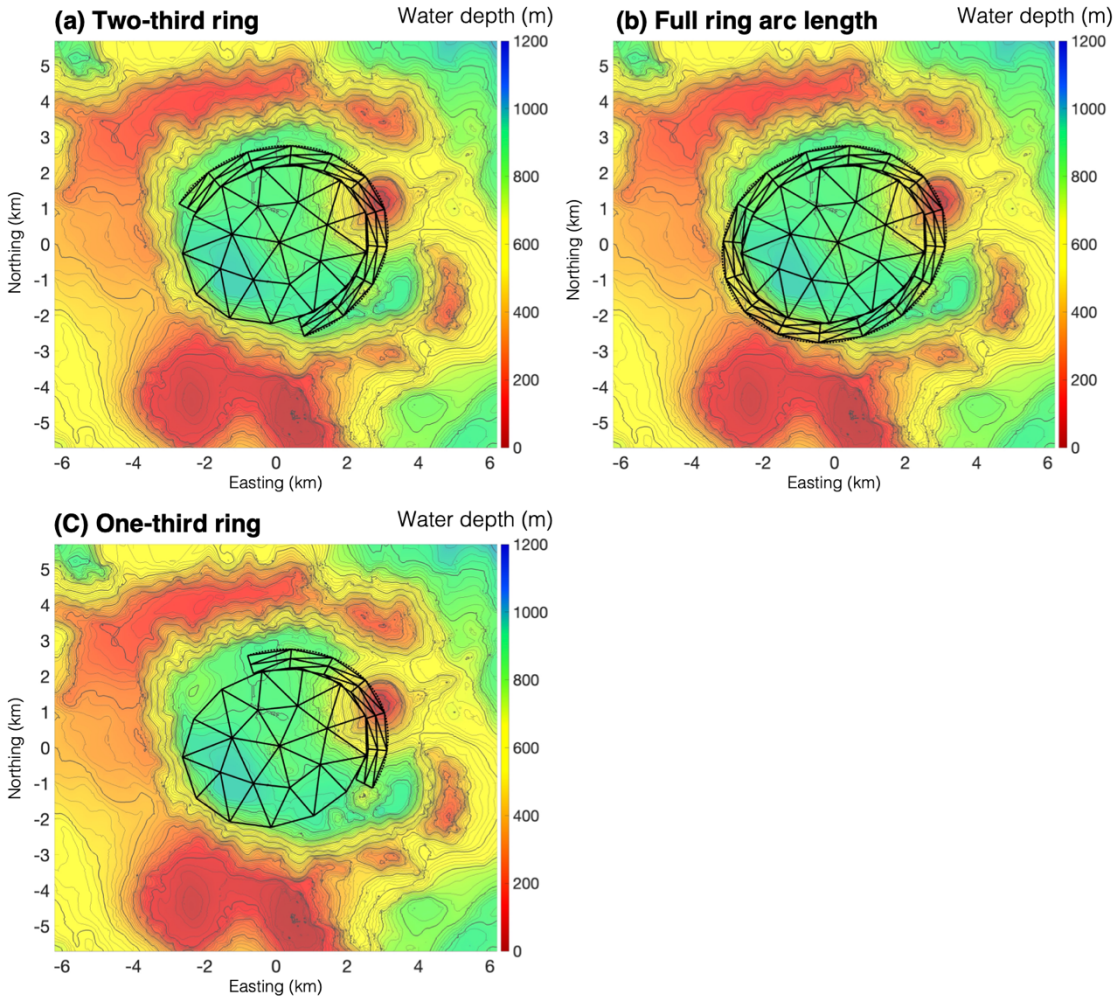

Figure S4. Three cases of the ring fault arc length assumed in the source modeling: (**a**) two-third ring, (**b**) full ring, and (**c**) one-third ring arc lengths.

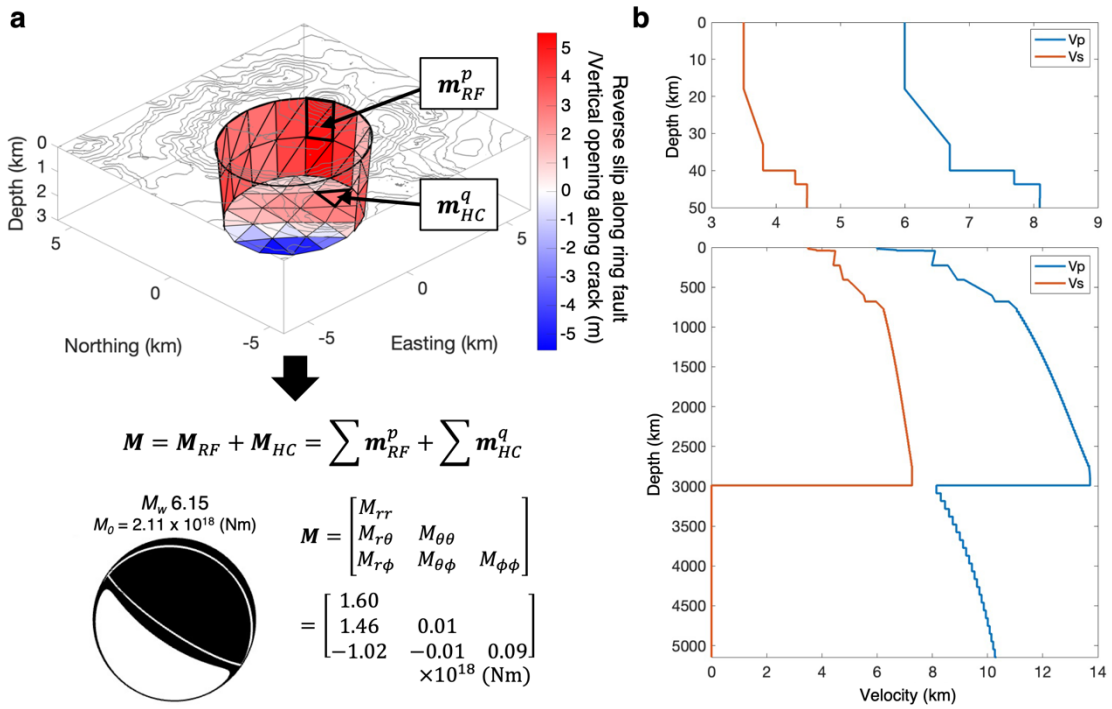

Figure S5. Moment tensor computation and 1-D velocity structure. (**a**) Moment tensor computation process. As an example, the case of the best-fit source model is shown (Figure 3b). (**b**) 1-D velocity structure used in this study (bottom panel). In the top panel, the velocities down to a depth of 50 km are shown.

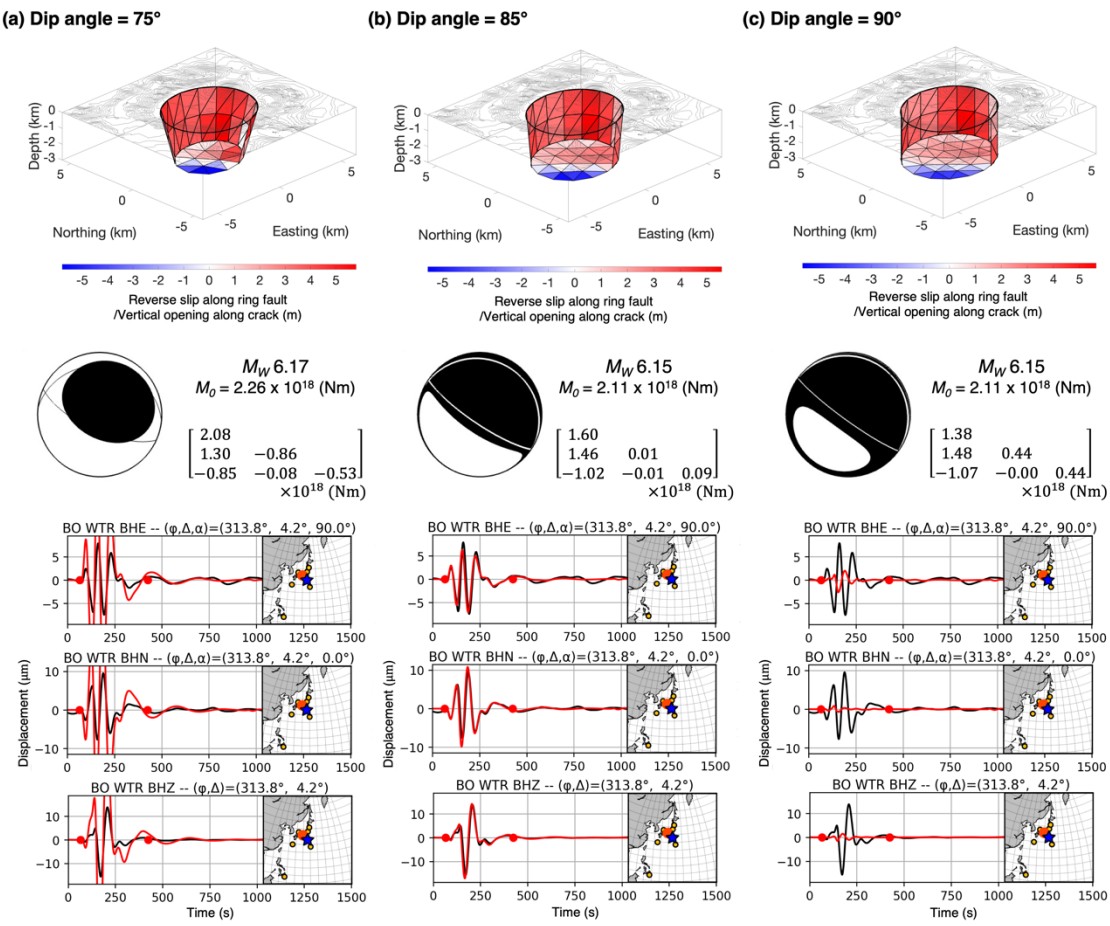

Figure S6. Comparison of source models with different ring fault dip angles: (**a**) 75.0°, (**b**) 85.0°, and (**c**) 90.0°. From top, trapdoor faulting motion, moment tensor, and synthetic seismograms of the models are shown. The ring fault has the two-third ring arc length, in all the cases. Note that amplitudes of synthetic seismic waveforms (red) from the models become smaller as the dip angle becomes steeper, despite their similar moment magnitudes.

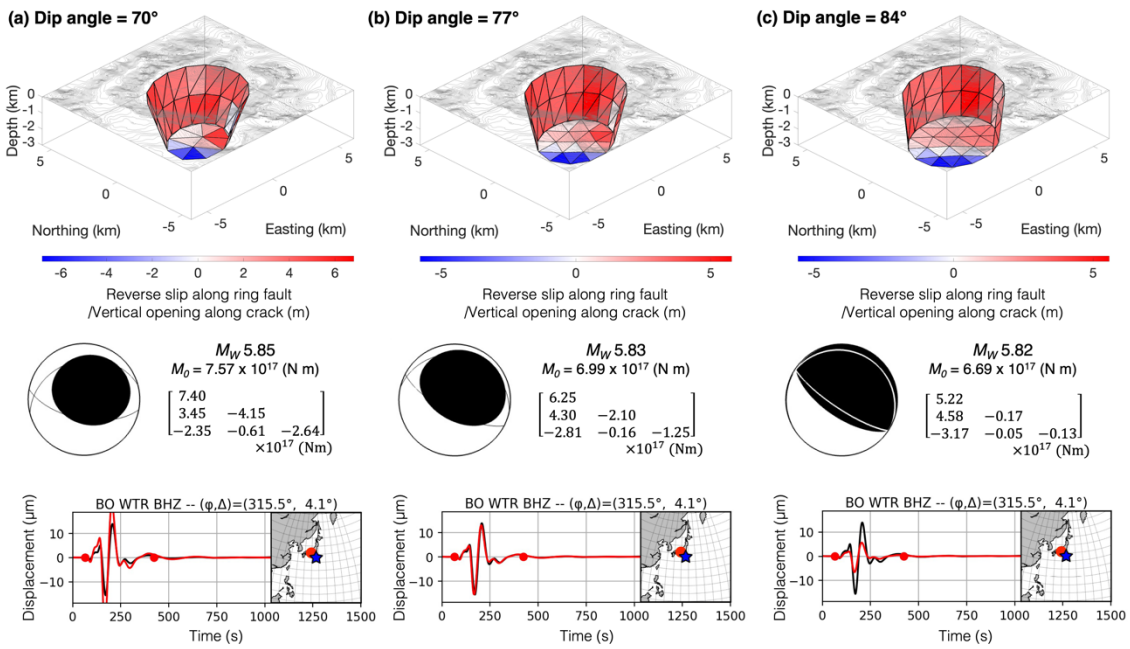

Figure S7. Synthetic long-period seismic waveforms when we assume low velocity (and low rigidity) at the shallowest depth < 5 km in the crust. The ring fault dip angles of the three models are (**a**) 70°, (**b**) 77°, and (**c**) 84°, respectively. From top, trapdoor faulting motion, moment tensor, and an example of synthetic seismic waveforms are shown. For descriptions, see Text S2.

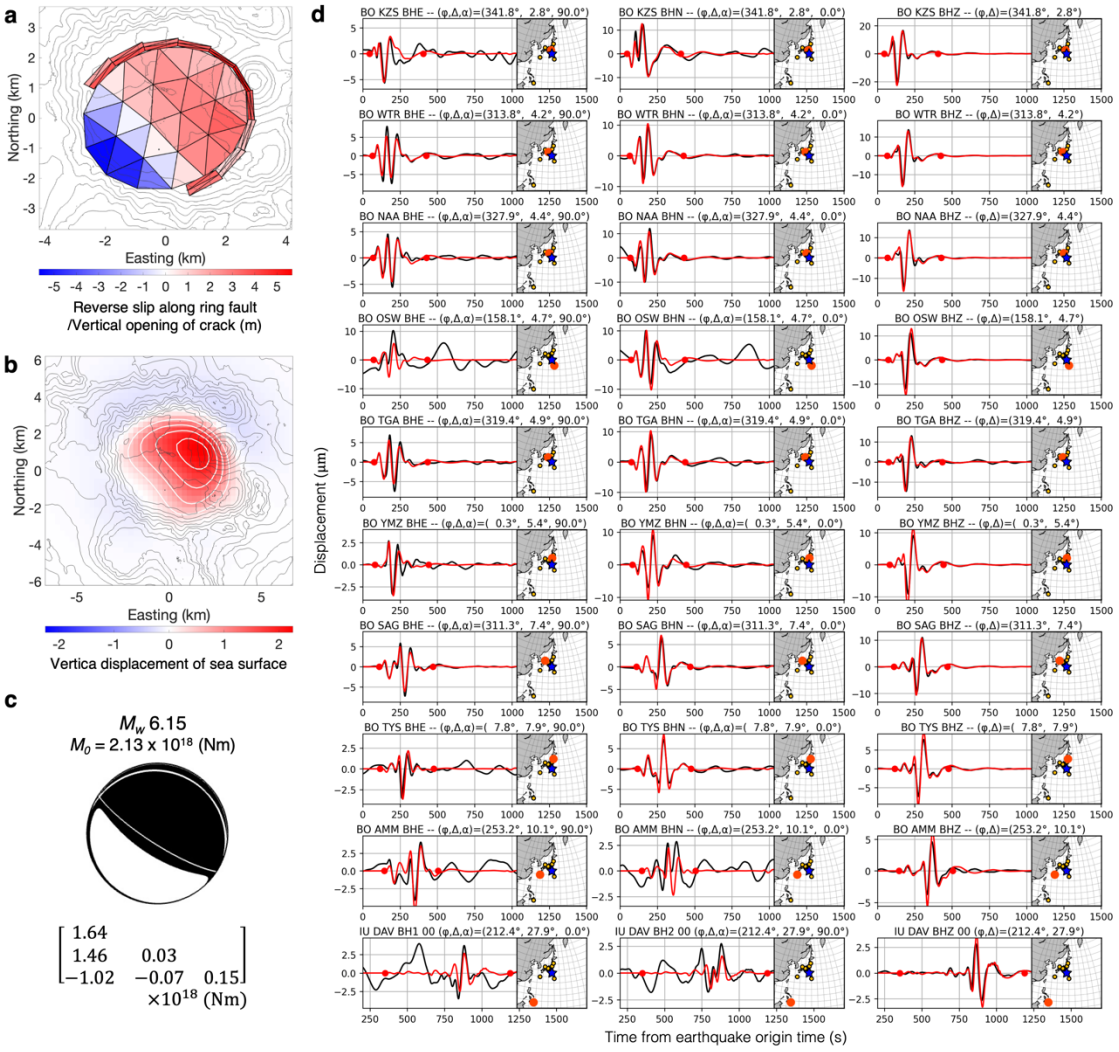

Figure S8. Source model with the modified ring fault dip angles (83°–87°). (**a**) Trapdoor faulting motion. Color representation follows that of Figure 3b. (**b**) Vertical sea-surface displacement caused by the model. Color representation follows that of Figure 5a. (**c**) Moment tensor of the model. (**d**) Comparison of the observed (black) and synthetic (red) long-period seismic waveforms (period = 60–250 s) from the model at representative stations. See the caption of Figure 6c. For detailed descriptions, see Text S3.

Event	Date (Y/M/D)	Time (h:m:s)	Longitude	Latitudes	Depth (km)	M_W	M_S
1	1984/6/13	2:29:29	139.93°	31.39°	15.2	5.6	5.4
2	1996/9/4	18:16:07	140.06°	31.48°	24.4	5.7	5.1
3	2006/1/1	7:12:07	140.07°	31.51°	12	5.6	5.0
4	2015/5/2	16:50:50	139.94°	31.47°	12	5.7	5.7
5	2018/5/6	6:04:06	139.98°	31.51°	12	5.4	5.4

Table S1. Earthquake information of volcanic earthquakes at Sumisu caldera, reported by the GCMT catalog (Ekström, Nettles, and Dziewoński 2012). Note that shallow source depths cannot be determined accurately with long-period seismic data used for the catalogue.

Network	Station code	Distance (degree)	Azimuth (degree)
F-net	KZS	2.82	344.57
F-net	JIZ	3.54	345.74
F-net	KNY	3.77	334.25
F-net	WTR	4.11	315.49
F-net	SGN	4.12	347.31
F-net	KIS	4.24	305.17
F-net	NAA	4.36	329.6
F-net	KMT	4.43	300.79
F-net	TTO	4.63	340.16
F-net	TSK	4.72	0.36
F-net	OSW	4.75	156.29
F-net	NOK	4.78	305.26
F-net	TGA	4.82	320.88
F-net	KNM	4.85	331.16
GSN	MAJO	5.28	343.59
F-net	YMZ	5.43	1.62
F-net	UMJ	5.49	293.93
F-net	SRN	5.5	329.74
F-net	YZK	5.9	309
F-net	WJM	6.41	337.87
F-net	KSK	6.77	3.54
F-net	NSK	7.34	294.95
F-net	SAG	7.36	312.11
F-net	TKO	7.53	275.4
F-net	KSN	7.57	8.77
F-net	TYS	7.97	8.64
F-net	KYK	8.36	264.9
F-net	SBR	8.52	286.26
F-net	IZH	9.5	289.03
F-net	TMR	9.66	6
F-net	AMM	9.91	253.18
F-net	KMU	10.98	11.41
GSN	TATO	17.58	252.97
GSN	GUMO	18.35	164.98
GSN	DAV	27.8	212.13
GSN	MA2	29	11.26

Table S2. Stations used for the computation of the long-period seismic waves. Station list of broad-band seismic stations used for the forward simulation of long-period seismic waves. For each station, we use the record of the three components.

Event	M_w	M_0 (x 10^{18} N m)	Moment tensor (x 10^{18} N m)						Half duration (s)
			M_{rr}	$M_{\theta\theta}$	$M_{\phi\phi}$	$M_{r\theta}$	$M_{r\phi}$	$M_{\theta\phi}$	
1996	5.99	1.20	0.384	-0.221	-0.164	0.282	-1.140	-0.069	5.3
2006	5.88	0.82	0.286	-0.189	-0.097	-0.159	-0.780	-0.024	8.0
2015	6.01	1.30	0.385	-0.225	-0.160	-0.311	-1.226	-0.071	5.0
2018	5.58	0.28	0.103	-0.091	-0.011	-0.107	-0.252	-0.006	4.0

Table S3. Results of the moment tensor analysis. Moment magnitudes, scalar seismic moments, moment tensors, and half durations of the repeating earthquakes. Note that $M_{r\theta}$ and $M_{r\phi}$ determined from long-period seismic waveforms are unreliable due to shallow source depths (Sandanbata et al. 2021).

Data Set S1. Source models of the trapdoor faulting (separate file). This dataset includes two source models presented in Figure 3b, and Figure S8.

Supplementary References

Duputel, Zacharie, Luis Rivera, Hiroo Kanamori, and Gavin Hayes. 2012. "W Phase Source Inversion for Moderate to Large Earthquakes (1990–2010)." *Geophysical Journal International* 189 (2): 1125–47.

Ekström, Göran, M. Nettles, and Adam M. Dziewoński. 2012. "The Global CMT Project 2004–2010: Centroid-Moment Tensors for 13,017 Earthquakes." *Physics of the Earth and Planetary Interiors* 200–201 (June): 1–9.

Hayes, Gavin P., Luis Rivera, and Hiroo Kanamori. 2009. "Source Inversion of the W-Phase: Real-Time Implementation and Extension to Low Magnitudes." *Seismological Research Letters* 80 (5): 817–22.

Kanamori, Hiroo, and Luis Rivera. 2008. "Source Inversion of Wphase: Speeding up Seismic Tsunami Warning." *Geophysical Journal International* 175 (1): 222–38.

Kodaira, Shuichi, Takeshi Sato, Narumi Takahashi, Aki Ito, Yoshihiko Tamura, Yoshiyuki Tatsumi, and Yoshiyuki Kaneda. 2007. "Seismological Evidence for Variable Growth of Crust along the Izu Intraoceanic Arc." *Journal of Geophysical Research* 112 (B5). https://doi.org/10.1029/2006jb004593.

Sandanbata, Osamu, Hiroo Kanamori, Luis Rivera, Zhongwen Zhan, Shingo Watada, and Kenji Satake. 2021. "Moment Tensors of Ring-Faulting at Active Volcanoes: Insights into Vertical-CLVD Earthquakes at the Sierra Negra Caldera, Galápagos Islands." *Journal of Geophysical Research, [Solid Earth]* 126 (6): e2021JB021693.